High-Performance Planar Solar Cells Based On $CH_3NH_3PbI_{3-x}Cl_x$ Perovskites with Determined Chlorine Mole Fraction

Yunlong Li, Weihai Sun, Weibo Yan, Senyun Ye, Haitao Peng, Zhiwei Liu, Zuqiang Bian,* and Chunhui Huang*

Solution-processable hybrid perovskite solar cells are a new member of next generation photovoltaics. In the present work, a low-temperature two-step dipping method is proposed for the fabrication of $CH_3NH_3PbI_{3-x}Cl_x$ perovskite films on the indium tin oxide glass/poly(3,4-ethylenedioxythiophene):poly(styrene sulfonate) (PEDOT:PSS) substrate. The bandgaps of the $CH_3NH_3PbI_{3-x}Cl_x$ perovskite films are tuned in the range between 1.54 and 1.59 eV by adjusting the $PbCl_2$ mole fraction ($n_{Cl}/(n_{Cl}+n_I)$) in the initial mixed precursor solution from 0.10 to 0.40. The maximum chlorine mole fraction measured by a unique potentiometric titration method in the produced $CH_3NH_3PbI_{3-x}Cl_x$ films can be up to 0.220 ± 0.020 ($x = 0.660 \pm 0.060$), which is much higher than that produced by a one-step spin-coating method (0.056 ± 0.015, $x = 0.17 \pm 0.04$). The corresponding solar cell with the $CH_3NH_3PbI_{2.34\pm0.06}Cl_{0.66\pm0.06}$ perovskite film sandwiched between PEDOT:PSS and C_{60} layers exhibits a power conversion efficiency as high as 14.5%. Meanwhile, the open-circuit potential (V_{oc}) of the device reaches 1.11 V, which is the highest V_{oc} reported in the perovskite solar cells fabricated on PEDOT:PSS so far.

1. Introduction

Perovskite, named after Russian geologist Perovski, initially referred to $CaTiO_3$ materials. Nowadays, all materials that have a generic chemical formula of ABX_3 and a cubic structure are defined as perovskites. Alternatively, the inorganic cation A in the perovskites can be replaced by suitable organic species, resulting in so-called hybrid perovskites.[1–6] The hybrid perovskites have been extensively studied due to their unique structural, optical,[1,2] electrical,[3,4] and magnetic[5] properties. Recently, hybrid perovskites with intriguing photovoltaic properties have been developed. For instance, $CH_3NH_3PbI_3$ ($MAPbI_3$) perovskite arouses wide interest because of its high optical absorption, high extinction coefficient in a broad wavelength range from visible to near infrared, and high carrier mobility.[7,8] In the past few years, these perovskite-structured organometal halides have been successfully applied in mesoporous solar cells (MSSCs),[9–15] where electrons can transfer rapidly from the hybrid perovskite to the mesoporous layer in the solar cells.[16] In addition, these perovskite materials can also be implemented in a planar heterojunction p-i-n architecture without mesoporous layer because of their ambipolar transport properties.[17–21] The large diffusion length (L_D) of the holes and electrons in perovskites can maintain or improve the performance of the planar heterojunction solar cells. The L_D is about 100 nm in $MAPbI_3$[22] and can be up to 1 μm in $CH_3NH_3PbI_{3-x}Cl_x$ ($MAPbI_{3-x}Cl_x$) perovskites.[23] The long L_D of $MAPbI_{3-x}Cl_x$ perovskite makes it one of the most suitable materials for planar heterojunction solar cells and the application of $MAPbI_{3-x}Cl_x$ perovskite usually leads to a higher open-circuit voltage in photovoltaic devices.[24] Moreover, introduction of chlorine also plays an important role in improving film morphology of the perovskites.[25]

Various $MAPbI_{3-x}Cl_x$ perovskites have been developed and used as light absorbing material for photovoltaic devices. The $MAPbI_{3-x}Cl_x$ perovskite-based solar cell prepared by dual-source vapor deposition displayed a short-circuit current (J_{sc}) of 21.5 mA cm^{-2}, open-circuit voltage (V_{oc}) of 1.07 V, fill factor (FF) of 0.67, and a power conversion efficiency (PCE) as high as 15.4%.[17] The solution-processed fabrication of hybrid perovskites, by contrast, is more convenient for the mass production of perovskite solar cells. Several groups have reported their results of $MAPbI_{3-x}Cl_x$ based solar cells by a spin-coating method,[26–30] among which the highest PCE of 19.3% was obtained by Yang and co-workers.[28] $MAPbI_{3-x}Cl_x$ based solar

Y. Li, W. Sun, Dr. W. Yan, S. Ye, Dr. Z. Liu, Dr. Z. Bian, Dr. C. Huang
Beijing National Laboratory for Molecular Science
State Key Laboratory of Rare Earth Materials and Applications
College of Chemistry and Molecular Engineering
Peking University
Beijing 100871, P.R. China
E-mail: zwliu@pku.edu.cn; bianzq@pku.edu.cn
H. Peng
Department of Energy and Resources Engineering
College of Engineering
Peking University
Beijing 100871, P.R. China

DOI: 10.1002/adfm.201501289

© 2015 WILEY-VCH Verlag GmbH & Co. KGaA, Weinheim

cells have made a great progress the role of chlorine and exact composition of halide perovskites has been debated.[31] Bein and co-workers prepared $MAPbI_{3-x}Cl_x$ by controlling the amount of methylammonium chloride (MACl) added into the MAI immersion solution.[30] While the resulting devices with the structure of TiO_2/perovskite/Spiro-MeOTAD/Au exhibited a high power conversion efficiency up to 15%, the exact effect of chlorine is not clear since the chlorine content in the perovskites is too small to measure. Some groups have studied the chlorine doping content in the $MAPbI_{3-x}Cl_x$ perovskites by X-ray photoelectron spectroscopy (XPS) or SEM energy-dispersive X-ray spectroscopy (EDS).[26,32,33] However, both EDS and XPS are not exactly measuring methods for obtaining the accurate chlorine doping content. Thus, it is necessary to find a better method to measure the chlorine doping content accurately for exploring the exact effect of chlorine in the $MAPbI_{3-x}Cl_x$ perovskites.

In the present work, a two-step dipping method is proposed for the fabrication of $MAPbI_{3-x}Cl_x$ films on poly(3,4-ethy lenedioxythiophene):poly(styrene sulfonate) (PEDOT:PSS). The obtained films were regular crystalline grains with a uniform morphology and showed full coverage on the PEDOT:PSS substrate. The bandgap of the $MAPbI_{3-x}Cl_x$ materials were tuned by changing the $PbCl_2$ mole fraction in the precursor solution from 0.10 to 0.40, and the corresponding chlorine mole fraction ($n_{Cl}/(n_{Cl} + n_I)$) was successfully measured by a potentiometric titration method. This is the first time to measure the accurate chlorine doping content in $MAPbI_{3-x}Cl_x$ perovskites so far. The corresponding solar cells with an inverted structure of ITO/PEDOT:PSS/$MAPbI_{3-x}Cl_x$/C_{60}/BCP/Ag were fabricated. The best device showed PCE, V_{oc}, J_{sc}, and FF of 14.5%, 1.11 V, 17.8 mA cm^{-2}, and 0.734, respectively.

2. Results and discussion

To investigate the effect of doping ratio of chlorine on their optical and electronic properties, a series of $MAPbI_{3-x}Cl_x$ perovskites were synthesized with chlorine mole fractions of 0.10, 0.20, 0.30, and 0.40 in the initial precursor solution. As the solubility of $PbCl_2$ in DMF is poor (this is the reason why we could not rise the chlorine mole fraction higher than 0.40 in the initial precursor solution), PbI_2 was used to facilitate the dissolution of $PbCl_2$ in *N*,*N*-dimethylformamide (DMF). The total concentration of PbI_2 and $PbCl_2$ was 1.5 M and used for all tests.

The X-ray diffractometer (XRD) peaks of all four $MAPbI_{3-x}Cl_x$ perovskites with different chlorine mole fractions were found at 14.16°, 28.50°, and 43.22°, which are ascribed to their (110), (220), and (330) lattice planes (**Figure 1**a). This result indicates the tetragonal structure of these perovskites, which conforms to the previously reported results.[34] The (110) plane diffraction peak of $CH_3NH_3PbCl_3$ was not observed at 15.68° while no $PbCl_2$ diffraction peaks were found in the XRD spectra (Figure 1b), indicating that the reaction of $PbCl_2$ with

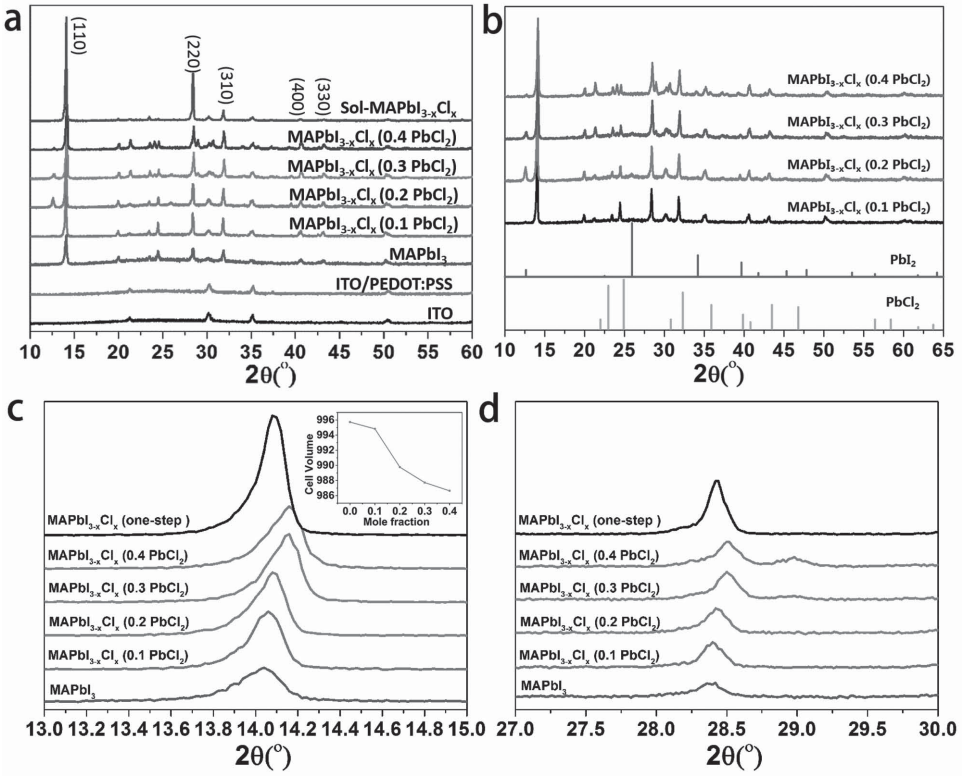

Figure 1. a) XRD pattern of ITO substrate, ITO/PEDOT:PSS and a series of $MAPbCl_xI_{3-x}$ perovskite films on ITO/PEDOT:PSS substrate fabricated with $PbCl_2$ mole fractions of 0.10, 0.20, 0.30, and 0.40 in the precursor solution. b) The simulated XRD pattern of $PbCl_2$, PbI_2 and measured XRD pattern of $MAPbCl_xI_{3-x}$ perovskite films on ITO/PEDOT:PSS substrate. c) Zoom-in of the XRD pattern at (110) lattice plane in (a). Insert is the change of the cell volume as a function of $PbCl_2$ mole fraction in the precursor. d) Zoom-in XRD pattern at (220) lattice plane in (a).

© 2015 WILEY-VCH Verlag GmbH & Co. KGaA, Weinheim

Table 1. Measured chlorine mole fraction in the perovskites corresponding to $PbCl_2$ mole fraction from 0.10 to 0.40 in the precursor, and comparison of prepared and measured chlorine mole fraction in standard I/Cl solutions.

$PbCl_2$ mole fraction in the precursor	Measured chlorine mole fraction in perovskites	Prepared chlorine mole fraction	Measured chlorine mole fraction
0.10	0.012 ± 0.008	0.0100	0.006
0.20	0.073 ± 0.012	0.0600	0.059
0.30	0.185 ± 0.015	0.2000	0.193
0.40	0.220 ± 0.020	0.2400	0.233

methylammonium cation was complete and a pure $MAPbI_{3-x}Cl_x$ phase was formed. Compared with the XRD pattern of $MAPbI_3$, the diffraction profile of $MAPbI_{3-x}Cl_x$ perovskite showed a similar pattern while it presents a slight difference in the lattice parameters. As seen from local XRD pattern (Figure 1c,d), an obvious shift could be seen in the strong (110) and (220) peaks. Although the shift is small, it is fairly above the instrumental sensitivity and is not negligible. The data fitting is shown in Table S1, Supporting Information, and these results indicate that $MAPbI_3$ was doped with a certain amount of chlorine. In addition, the sequential reduction of unit cell volume also indicates the increased chlorine content in these perovskites. Moreover, SEM EDS results show that different $PbCl_2$ mole fractions in initial precursor solution result in different chlorine doping extent in $MAPbI_{3-x}Cl_x$ films. The chlorine content in the mixed halide $MAPbI_{3-x}Cl_x$ film increased obviously with the increase of the $PbCl_2$ mole fraction in precursor solution from 0.1 to 0.4 (Figure S1, Supporting Information).

The XRD pattern showed that the chlorine doping content in our perovskites prepared by a two-step dipping method using the initial precursor solution of 0.30 or 0.40 chlorine mole fraction, is higher than that fabricated by a one-step method. As we know, it is difficult to get the accurate value of chlorine doping content in $MAPbI_{3-x}Cl_x$ films from the XRD pattern. Furthermore, it is also hard to get the accurate value by SEM EDS or XPS. Herein, the ingenious application of potentiometric titration method allows us to measure the chlorine content precisely. Since the chlorine content in the $CH_3NH_3I_{3-x}Cl_x$ perovskites is relatively small, extra chlorine was added in the solution for making it better to tell the second titration end point apart from the first, i.e., titration end point of chlorine apart from iodine. To deduct the additional chlorine in the prepared solution, we carried out blank experiment three times. The titration curves of the blank experiment were shown in Figure S2, Supporting Information. The three titrimetric results (1.079, 1.081, 1.068 mL) showed that it was relatively precise with a small relative error (<1%). Figure S3, Supporting Information, shows the titration curves of the prepared sample solutions. The detailed chlorine mole fractions of the perovskites films fabricated with $PbCl_2$ mole fraction from 0.10 to 0.40 in the precursor are summarized in **Table 1**. Detailed calculation processes could be found in the Supplementary Information. To verify the precision of the proposed titration method, a series of standard I/Cl mixed solutions were prepared. The chlorine mole fraction of the standard solutions was 0.0100, 0.0600, 0.2000, and 0.2400, respectively. Applying the same method, we titrated each of the standard I/Cl mixed solution in turn. The titration curves of these samples were shown in Figure S4, Supporting Information, and the corresponding measured results were summarized in Table 1. Data show that the results given by the proposed method are in well agreement with what we have prepared, which confirmed the accuracy of the titration method we proposed. By the way, the perovskites formed by a one-step method were also fabricated in our experiments, and the perovskites were titrated by the same method as well. The chlorine mole fraction in the perovskites fabricated by the one-step method is 0.056 ± 0.015, which is close to the value that fabricated by the two-step method with a precursor solution containing 0.20 mole fraction of $PbCl_2$. And similar results could also be found in the XRD pattern (Figure 1c,d). The difference between our results and the reported ones may arise from different fabrication methods of the perovskite layer. In Angelis's work, the low chlorine content may due to a high annealing temperature,[35] as it is known that chlorine in perovskite would react with MA^+ to be MACl, which could diffuse out from bulk to interface easily at high temperature with long time.[33] Furthermore, chlorine content up to 25.9% has been demonstrated without annealing the perovskite in Hodes's work.[33] Moreover, in most reported work that having low chlorine content the $MAPbI_{3-x}Cl_x$ layer was fabricated by a one-step method. Our study indicates that a higher chlorine content can be achieved in a two-step method. The reported work with the $MAPbI_{3-x}Cl_x$ perovskite fabricated by the two-step method that same to us showed also high chlorine content in the perovskites.[29]

The visual absorption spectra of the perovskite films showed a blue-shift in the bandgap with the increase of $PbCl_2$ mole fraction in precursor solution (**Figure 2**a). Extrapolated from the absorption of direct transition at absorption edge, the bandgap of the $MAPbI_{3-x}Cl_x$ perovskites was tuned from 1.54 eV (absorption edge at 801 nm) to 1.59 eV (absorption edge at 782 nm) with increase of $PbCl_2$ mole fraction in the precursor solution

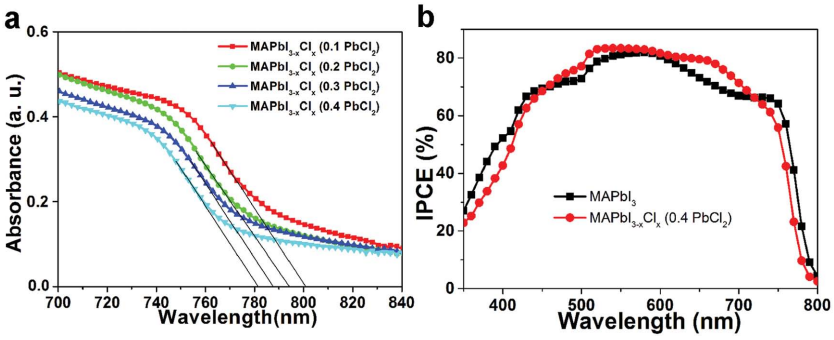

Figure 2. a) Visible absorption spectra of the $MAPbI_{3-x}Cl_x$ films fabricated with $PbCl_2$ mole fractions of 0.10, 0.20, 0.30, and 0.40 in precursor solution with a thickness around 300 ± 15 nm. b) The IPCE spectrum of the planar heterojunction solar cell fabricated with chlorine and without chlorine.

© 2015 WILEY-VCH Verlag GmbH & Co. KGaA, Weinheim

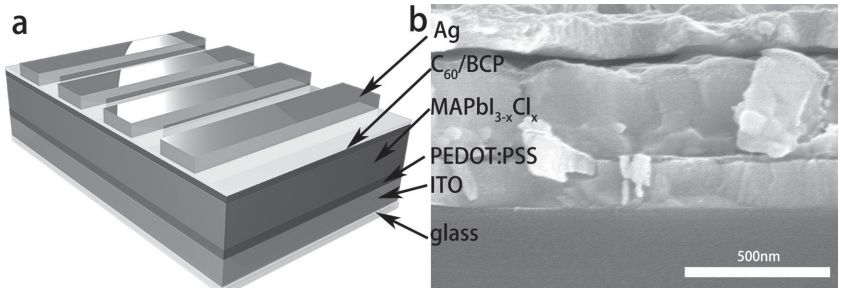

Figure 3. a) Configuration diagram of the $MAPbI_{3-x}Cl_x$ perovskite hybrid solar cell in this work; b) The cross-sectional SEM image of the solar cell with a layer structure of ITO/PEDOT:PSS/$MAPbI_{3-x}Cl_x$/C_{60}/BCP/Ag. The thickness of the $MAPbI_{3-x}Cl_x$ film is around 300 ± 15 nm.

from 0.10 to 0.40. The large background in absorption was then taken into consideration, which makes the application of regular absorption spectra for bandgap evaluation may be not good enough. Thus, we supplied the EQE data of the devices with chlorine and without chlorine in Figure 2b. The EQE band edge of the device using 40% precursor solution was 775 nm while that of the device without chlorine was 796 nm. Both of absorption spectra and the EQE spectra demonstrated that the doped chlorine has increased the bandgap of the perovskites. It is found obviously that the EQE band edge shifts to short wavelength.

A series of devices with a layer structure of ITO/PEDOT:PSS/$MAPbI_{3-x}Cl_x$/C_{60}/BCP/Ag were constructed, where the $MAPbI_{3-x}Cl_x$ perovskite was used as light harvester, PEDOT:PSS layer was used as hole transport material (HTM) and C_{60} was used as electron transport material (ETM) (**Figure 3**a) and its cross-sectional SEM image is shown in Figure 3b. The $MAPbI_{3-x}Cl_x$ perovskite layer was prepared by PbI_2/$PbCl_2$ mixed precursor solution with 0.10, 0.20, 0.30 or 0.40 $PbCl_2$ mole fractions with the thicknesses around 300 ± 15 nm. The photovoltaic parameters of the corresponding solar cells are summarized in **Figure 4**. It is clear that the device parameters were increased with the increase of chlorine doping content. V_{oc} was increased from 1.00 to 1.09 V with the increase of $PbCl_2$ mole fraction in the precursor solution from 0.10 to 0.40, which might be attributed to the increased bandgap of the $MAPbI_{3-x}Cl_x$ perovskite with high chlorine doping content mostly. Regarding to the increased voltage, it is our point of view that the increased bandgap is one of the reasons. However, it is obviously, the increased voltage is larger than the increased bandgap. The possible reason we believe is the improved carrier diffusion length and charge mobility in the $MAPbCl_{3-x}I_x$ perovskites,[23] which would decrease series resistance and the exciton recombination in the devices. Thus, it would not only have a positive effect on the V_{oc}, but also on the photocurrent density and FF. The best device in the experiment was based on the 0.40 mole fraction $PbCl_2$ precursor, and the corresponding current density–voltage (*J*–*V*) is shown in **Figure 5**a. The J_{sc}, V_{oc}, FF, and PCE of the solar cell are 17.8 mA cm^{-2}, 1.11 V, 0.734, and 14.5% by a forward scan mode (–0.5 to 1.5 V) and 18.0 mA cm^{-2}, 1.10 V, 0.707, and 14.0% by a reverse scan mode (1.5 to –0.5 V), respectively. The *J*–*V*

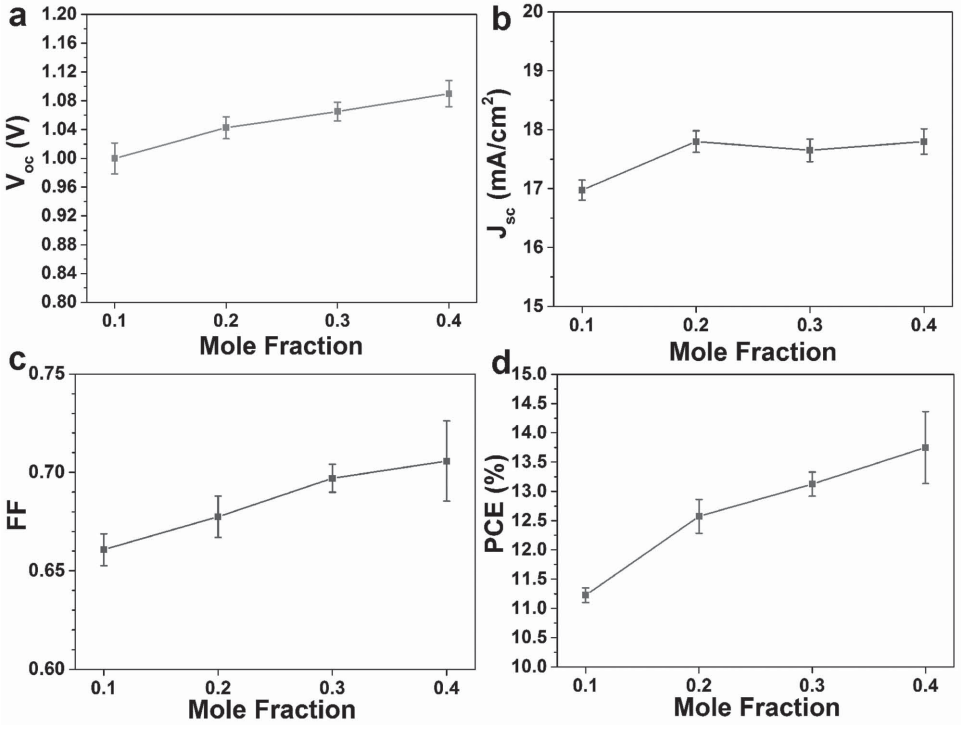

Figure 4. The photovoltaic parameters of the $MAPbI_{3-x}Cl_x$ perovskite solar cells fabricated with different $PbCl_2$ mole fractions in the precursor solution. a) V_{oc} b) J_{sc} c) FF d) PCE.

© 2015 WILEY-VCH Verlag GmbH & Co. KGaA, Weinheim

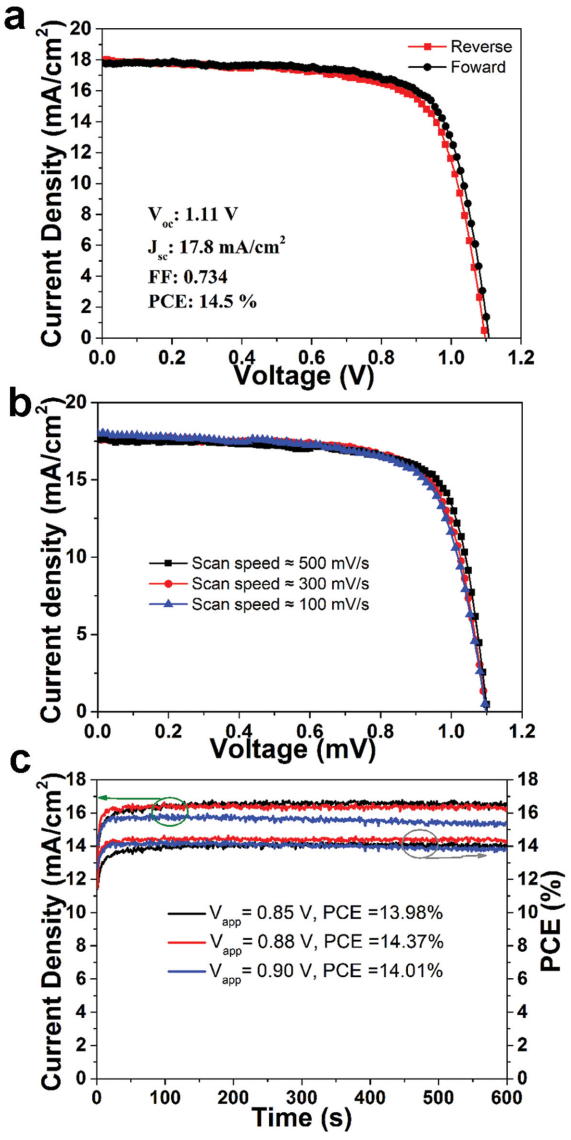

Figure 5. a) The current density–voltage (*J–V*) curves of the best solar cell fabricated with two-step dipping method under the simulation of AM 1.5G, 100 mW cm^{-2}. b) *J–V* curves obtained at different scanning rates (100 to 500 mV s^{-1}). c) The steady photocurrent output measured under different bias potentials and continuous light illumination.

curves of the best cell obtained at different scanning rates from 100 to 500 mV s^{-1} are shown in Figure 5b. The detected efficiencies are very close, reflecting that the solar cell reaches an equilibrium state and its output should be very close to the real value. Furthermore, the steady photocurrent output measured under different bias potentials and continuous light illumination are shown in Figure 5c. The equilibrium photocurrent densities generated at 0.850, 0.880, and 0.900 V are 16.45, 16.33, and 15.57 mA cm^{-2}, respectively. Accordingly, the calculated solar conversion efficiencies are 13.98%, 14.37%, and 14.01%, respectively. To the best of our knowledge, this is the highest efficiency reported so far for the $MAPbI_{3-x}Cl_x$ perovskite in an inverted structure of PEDOT:PSS/$MAPbI_{3-x}Cl_x$. The $MAPbI_{3-x}Cl_x$ planar heterojunction solar cell also exhibited high incident photon-to-electron conversion efficiency (IPCE) in a broad visible absorption range up to 775 nm (Figure 2b). The highest IPCE reached 83%, which was obtained at 530 nm with an optical bandgap of 1.59 eV. The integration of the IPCE spectrum with an AM 1.5G solar photon flux yielded a current density of 17.8 mA cm^{-2}, which is consistent with the measured photocurrent density. The reproducibility of the perovskite-based photovoltaics was well demonstrated by 15 separate devices, which were fabricated and characterized as described above. Their photovoltaic parameters are presented in Table S2, Supporting Information.

A comparison between the $MAPbI_{3-x}Cl_x$ films fabricated by two-step dipping method described in the present work and the conventional one-step spin-coating were conducted. As shown in **Figure 6**, the film fabricated via two-step dipping method displayed a complete coverage with regular crystalline grains while the other showed a lower surface coverage. In addition, the perovskites film fabricated by the two-step dipping method is smoother than that made by the one-step spin-coating method. Their average roughness is 45 and 105 nm, respectively, which was measured by atomic force microscope (AFM) (Figure S5, Supporting Information). The performance parameters of the corresponding solar cells fabricated using two-step deposition and one-step spin-coating method are summarized in **Table 2**. The devices fabricated with two-step dipping method showed a slightly lower J_{sc}, but much higher V_{oc} and FF. The lower J_{sc} may be attributed to the lower crystallinity of the perovskite fabricated by two-step dipping method (Figure 1), which results in a higher series resistance (R_s) of the devices. The full coverage and high chlorine doping content of the perovskite film reduce its leakage current[19,36] and increase the bandgap, respectively, which results in the higher V_{oc}. In addition, the high parallel resistance, resulted from the fully covered perovskite layer fabricated with the two-step dipping method on PEDOT:PSS film in devices, accounts for the larger FF of the corresponding solar cell.

3. Conclusions

A two-step dipping method for the fabrication of $MAPbI_{3-x}Cl_x$ (x = 0.036 ± 0.024–0.660 ± 0.060) perovskite layer on a flat

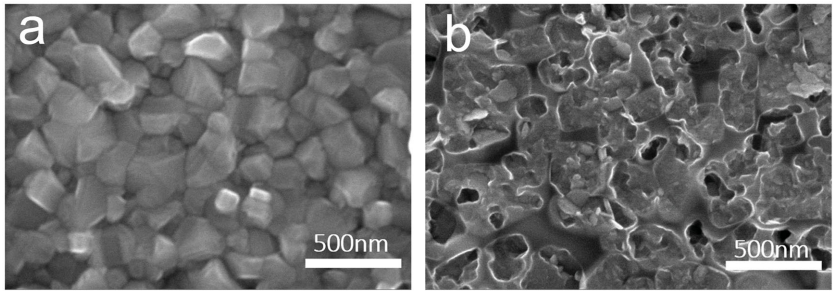

Figure 6. The SEM images of the disparate perovskite layers fabricated by a) two-step dipping method and b) one-step spin-coating deposition.

© 2015 WILEY-VCH Verlag GmbH & Co. KGaA, Weinheim

Table 2. Performance parameters of solar cells with $MAPbCl_xI_{3-x}$ perovskite film fabricated under the same conditions other than the fabricated method of perovskites.

Fabrication method	J_{sc} [mA cm^{-2}]	V_{oc} [V]	FF	PCE [%]	R_s [Ω cm^2]	R_{sh} [KΩ cm^2]
One-step	18.6 ± 0.04	1.00 ± 0.02	0.59 ± 0.02	11.0 ± 0.05	6.0 ± 0.1	0.6 ± 0.2
Two-step	17.7 ± 0.03	1.09 ± 0.02	0.71 ± 0.02	13.7 ± 0.08	7.5 ± 0.1	2.4 ± 0.2

substrate (ITO/PEDOT:PSS) was demonstrated. The chlorine content was determined with a small absolute error (<0.020) using a quantitative analysis method: potentiometric titration. The bandgap of the perovskite can be tuned from 1.54 to 1.59 eV by changing the chlorine doping content. The perovskites fabricated by this two-step dipping method showed better morphology and coverage than that prepared using the conventional one-step method, leading to a much higher V_{oc} and FF of the corresponding solar cell. The solar cell with the $CH_3NH_3PbI_{2.34\pm0.06}Cl_{0.66\pm0.06}$ perovskites as light harvester showed a PCE up to 14.5% and a V_{oc} as high as 1.11 V under AM1.5G illumination.

4. Experimental section

Materials: Methylamine (25% solution) and hydroiodic acid (45% solution) were purchased from Sinopharm Chemical Reagent Co., Ltd (Shanghai, China). Methylammonium iodide (CH_3NH_3I) was synthesized by the reaction of methylamine with hydroiodic acid as previously reported.[24] Raw materials used to prepare CH_3NH_3I are methylamine (CH_3NH_2) (25% in water, Sinopharm Chemical Reagent Co., Ltd.) and hydroiodic acid (HI) (45% in water, Sinopharm Chemical Reagent Co., Ltd.). Poly(3,4-ethylenedioxythiophene):poly(styrene sulfonate) (PEDOT:PSS) (Clevious P VP AI 4083), PbI_2 (99.9985%), $PbCl_2$ (99.99%), C_{60} (99.9%) and 2,9-dimethyl-4,7-diphenyl-1,10-phenanthroline (BCP) (98%) were purchased from H. C. Stark Company, Alfa Aesar, Aladdin, Puyang Yongxin Fullerene Technology Co. Ltd and Acros Organics, respectively. BCP was purified by thermal gradient sublimation before use. All other materials were used without any further purification. ITO (8 Ω sq^{-1}) coated glass substrate was obtained from Huayulianhe Co., Ltd.

Potentiometric Titration: First, we fabricated a series of perovskites using precursor solution with $PbCl_2$ mole fraction from 0.10 to 0.40 on ITO glass/PEDOT:PSS substrates. Then we loaded these perovskites with 250 mL ultrapure water in a beaker. Though an approximately calculation (see the Supporting Information), each substrate has about 10^{-6} mole iodine and 10^{-7} mole chlorine. Since the solubility products (K_{sp}) of PbI_2 and $PbCl_2$ are 7.1×10^{-9} and 1.6×10^{-5}, respectively, these perovskites can be well dissolved. After that, 0.01 M $AgNO_3$ solution was used to titrate those perovskites solution by a ZDJ-4A automatic potentiometric titrator. During which 10.00 mL 1.000×10^{-3} M NaCl (primary standard) was added in the prepared solution since the inherent chlorine content in perovskite films is too small to separate the titration end point of chlorine from iodine. The titration rate was 0.080 mL min^{-1}. The titration end points are determined by the instrument automatically. Based on Nernst equation, the $Ag^{\pm}$/Ag electrode potential changes because of the changing of $Ag^{\pm}$ concentration during the titration process. When a titration end point is reached, the potential (E)–volume (V) curve would appear a turning point (the largest value of dE/dV), which can be recorded by the instrument.

Device Fabrication: The ITO coated glass substrate was cleaned in an ultrasonic bath with detergent, deionized water, acetone and isopropyl alcohol sequentially for 20 min. The substrate was then treated in an ultraviolet-ozone environment for 10 min and spin-coated with PEDOT:PSS (filtered through a 0.45 μm filter) at 500 rpm for 9 s and 4000 rpm for 60 s. The PEDOT:PSS layer was dried in an oven at 140 °C for 20 min. The ITO/PEDOT:PSS substrate was then spin-coated with a 1.5 M $PbI_2/PbCl_2$ precursor solution (dissolved at 85 °C and then cooled at room temperature before use) in DMF at 8000 rpm for 60 s at 20 °C and 20% humidity. The mole fractions of $PbCl_2$ ($n_{Cl}/(n_{Cl} + n_I)$) in the precursor solution were 0.10, 0.20, 0.30, and 0.40. The substrate was then air-dried, dipped into a preheated CH_3NH_3I solution (15 mg mL^{-1} in 2-propanol) for 60 s. Since the higher formation energy of chlorine incorporation into the perovskite matrix than that of iodine incorportation,[36] we chose the temperature of CH_3NH_3I solution 70 °C. After that, the formed perovskite layer was rinsed with 2-propanol and heated at 75 °C for 20 min. C_{60} (30 nm), BCP (8 nm), and Ag (100 nm) layers were sequentially deposited by thermal evaporation under vacuum (10^{-6} mbar). The active area of the devices was 0.100 cm^2.

Characterization: All photovoltaic measurements were carried out in air. An Oriel 300 W solar spectrum simulator (Thermo Oriel 91160–1000) with an AM 1.5G light filter was corrected with a standard Si solar cell to 100 mW cm^{-2} illumination intensity and used to obtain the emission spectra. All current-–voltage curves were recorded on a measuring system (Keithley Model 4200) by applying an external potential bias on the cell. The incident-photo-to-current conversion efficiency was recorded on a Keithley 2400 source meter under an irradiation of a 150 W tungsten lamp with a 1/4 m monochromator (Spectral Product DK 240). The optical absorption spectra were scanned with a UV-3100 spectrophotometer (Shimadzu, Japan). The crystallographic properties of $MAPbCl_xI_{3-x}$ films on the ITO/PEDOT:PSS substrates were investigated using a D/MAX-2000 X-ray diffractometer under monochromated Cu $K\alpha$ irradiation (λ = 1.5418 Å) at a scan rate of 4° min^{-1}. Scanning electron microscope (SEM) images were captured with a field emission scanning electron microscope (Hitachi S-4800) and atomic force microscope (SPI3800/SPA400 SPM, Seiko Instrument Inc.). The thickness of the films was measured using a KLA-Tencor Alpha-Step Surface Profiler. Potentiometric titration curves were captured by a ZDJ-4A automatic potentiometric titrator (Shanghai INESA Scientific Instrument Co., Ltd.),in which the input volume error can be accurately controlled in ±10 μL by a peristaltic pump.

Acknowledgements

The authors gratefully acknowledge the financial support from National Basic Research Program (2011CB933303) and National Natural Science Foundation of China (NSFC) (Grant Nos. 21321001 and 21371012).

Received: March 31, 2015
Revised: May 27, 2015
Published online: July 2, 2015

[1] D. B. Mitzi, C. D. Dimitrakopoulos, L. L. Kosbar, *Chem. Mater.* **2001**, *13*, 3728.
[2] M. Era, S. Morimoto, T. Tsutsui, S. Saito, *Appl. Phys. Lett.* **1994**, *65*, 676.
[3] D. B. Mitzi, C. A. Field, W. T. A. Harrison, A. M. Guloy, *Nature* **1994**, *369*, 467.

© 2015 WILEY-VCH Verlag GmbH & Co. KGaA, Weinheim

[4] C. R. Kagan, *Science* **1999**, *286*, 945.
[5] P. Zhou, J. E. Drumheller, B. Patyal, R. D. Willett, *Phys. Rev.* **1992**, *45*, 12365.
[6] D. B. Mitzi, *J. Chem. Soc., Dalton Trans.* **2001**, *1*, 1.
[7] A. Kojima, K. Teshima, Y. Shirai, T. Miyasaka, *J. Am. Chem. Soc.* **2009**, *131*, 6050.
[8] J. H. Im, C. R. Lee, J. W. Lee, S. W. Park, N. G. Park, *Nanoscale* **2011**, *3*, 4088.
[9] H. S. Kim, C. R. Lee, J. H. Im, K. B. Lee, T. Moehl, A. Marchioro, S. J. Moon, R. Humphry-Baker, J. H. Yum, J. E. Moser, M. Gratzel, N. G. Park, *Sci. Rep.* **2012**, *2*, 591.
[10] H. Li, K. Fu, A. Hagfeldt, M. Gratzel, S. G. Mhaisalkar, A. C. Grimsdale, *Angew. Chem. Int. Ed.* **2014**, *53*, 4085.
[11] J. Burschka, N. Pellet, S. J. Moon, R. Humphry-Baker, P. Gao, M. K. Nazeeruddin, M. Gratzel, *Nature* **2013**, *499*, 316.
[12] S. Ryu, J. H. Noh, N. J. Jeon, Y. C. Kim, W. S. Yang, J. Seo, S. I. Seok, *Energy Environ. Sci.* **2014**, *7*, 2614.
[13] N. J. Jeon, H. G. Lee, Y. C. Kim, J. Seo, J. H. Noh, J. Lee, S. I. Seok, *J. Am. Chem. Soc.* **2014**, *136*, 7837.
[14] D. Liu, T. L. Kelly, *Nat. Photonics* **2013**, *8*, 133.
[15] A. Yella, L. P. Heiniger, P. Gao, M. K. Nazeeruddin, M. Gratzel, *Nano Lett.* **2014**, *14*, 2591.
[16] A. Marchioro, J. Teuscher, D. Friedrich, M. Kunst, R. van de Krol, T. Moehl, M. Grätzel, J.-E. Moser, *Nat. Photonics* **2014**, *8*, 250.
[17] M. Liu, M. B. Johnston, H. J. Snaith, *Nature* **2013**, *501*, 395.
[18] J. Y. Jeng, Y. F. Chiang, M. H. Lee, S. R. Peng, T. F. Guo, P. Chen, T. C. Wen, *Adv. Mater.* **2013**, *25*, 3727.
[19] Q. Wang, Y. Shao, Q. Dong, Z. Xiao, Y. Yuan, J. Huang, *Energy Environ. Sci.* **2014**, *7*, 2359.
[20] Z. Xiao, C. Bi, Y. Shao, Q. Dong, Q Wang, Y. Yuan, C. Wang, Y. Gao, J. Huang, *Energy Environ. Sci.* **2014**, *7*, 2619.
[21] Y. Wu, A. Islam, X. Yang, C. Qin, J. Liu, K. Zhang, W. Peng, L. Han, *Energy Environ. Sci.* **2014**, *7*, 2934.
[22] G. Xing, N. Mathews, S. Sun, S. S. Lim, Y. M. Lam, M. Gratzel, S. Mhaisalkar, T. C. Sum, *Science* **2013**, *342*, 344.
[23] S. D. Stranks, G. E. Eperon, G. Grancini, C. Menelaou, M. J. Alcocer, T. Leijtens, L. M. Herz, A. Petrozza, H. J. Snaith, *Science* **2013**, *342*, 341.
[24] M. M. Lee, J. Teuscher, T. Miyasaka, T. N. Murakami, H. J. Snaith, *Science* **2012**, *338*, 643.
[25] S. T. Williams, F. Zuo, C. Chueh, C. Liao, P. Liang, A. K. Jen, *ACS Nano* **2014**, *8*, 10640.
[26] J. You, Z. Hong, Y. M. Yang, Q. Chen, M. Cai, T. B. Song, C. C. Chen, S. Lu , Y. Liu, H. Zhou, Y. Yang, *ACS Nano* **2014**, *8*, 1674.
[27] P. W. Liang, C. Y. Liao, C. C. Chueh, F. Zuo, S. T. Williams, X. K. Xin, J. Lin, A. K. Jen, *Adv. Mater.* **2014**, *26*, 3748.
[28] H. P. Zhou, Q. Chen, G. Li, S. Luo, T. Song, H. Duan, Z. Hong, J. You, Y. Liu, Y. Yang, *Science* **2014**, *345*, 542.
[29] Y. Ma, L. Zheng, Y. H. Chung, S. Chu, L. Xiao, Z. Chen, S. Wang, B. Qu, Q. Gong, Z. Wu, X. Houc, *Chem. Commun.* **2014**, *50*, 12458.
[30] P. Docampo, F. Hanusch, S. D. Stranks, M. Döblinger, J. M. Feckl, M. Ehrensperger, N. K. Minar, M. B. Johnston, H. J. Snaith, T. Bein, *Adv. Energy Mater.* **2014**, *4*, 1400355.
[31] E. Unger, A. Bowring, C. Tassone, V. Pool, A. Gold-Parker, R. Cheacharoen, K. Stone, E. Hoke, M. Toney, M. McGeheea, *Chem. Mater.* **2014**, *26*, 7158.
[32] H. Yu, F. Wang, F. Xie, W. Li, J. Chen,N. Zhao , *Adv. Funct. Mater.* **2014**, *24*, 7102.
[33] Y. Tidhar, E. Edri, H. Weissman, D. Zohar, G. Hodes, D. Cahen, B. Rybtchinski, S. Kirmayer, *J. Am. Chem. Soc.* **2014**, *136*, 13249.
[34] S. Colella, E. Mosconi, P. Fedeli, A. Listorti, F. Gazza, F. Orlandi, P. Ferro, T. Besagni, A. Rizzo, G. Calestani, G. Gigli, F. De Angelis, R. Mosca, *Chem. Mater.* **2013**, *25*, 4613.
[35] E. Mosconi, A. Amat, M. K. Nazeeruddin, M. Grätzel, F. De Angelis, *J. Phys. Chem. C* **2013**, *117*, 13902.
[36] G. E. Eperon, V. M. Burlakov, P. Docampo, A. Goriely, H. J. Snaith, *Adv. Funct. Mater.* **2014**, *24*, 151.

© 2015 WILEY-VCH Verlag GmbH & Co. KGaA, Weinheim